

REMOTE SENSING SCIENCE RESEARCH USING A SYSTEM SIMULATION¹

John P. Kerekes and David A. Landgrebe

Laboratory for Applications of Remote Sensing
and School of Electrical Engineering
Purdue University, West Lafayette, Indiana, USA

ABSTRACT

With the advent of configurable instruments such as SPOT, HIRIS, and MODIS, the need increases for continued research into the remote sensing process. A system model for this process is presented along with results from the application of this model to the study of parameter effects on the performance of a model sensor based on HIRIS.

Keywords: Remote Sensing Science, System Simulation, HIRIS Parameter Studies

1. INTRODUCTION

As we enter the era of configurable sensors for the remote sensing of the Earth's resources with the advent of such instruments as HIRIS (Goetz and Herring, 1989), and MODIS (Salomonson, et. al., 1989), the need increases for continued basic research into the remote sensing process. Earth scientists and other users of remotely sensed imagery will be increasingly called upon to specify conditions and parameters of the scene and sensor systems used to gather data for their experiments. While experience will continue to be the best tool for specifying such experiments, it is indeed worthwhile to develop in the literature an overall understanding of the remote sensing process from a scientific point of view.

A model for the remote sensing process has been developed and implemented as a simulation (RSSIM) to provide such a vehicle for exploring the interrelated effects of parameter choices. The approach chosen for this model has been one of looking at the remote sensing process as a system, and synthesizing a process-wide model that is based upon well developed component models. The system model is comprised of *scene* models including the reflectance of the surface and the atmospheric effects, *sensor* models including the spatial and spectral sampling effects and electrical noise, and *processing* algorithms including those for feature extraction or data compression and computing a resultant classification accuracy.

In Kerekes and Landgrebe (1988) we outlined the structure of this model. In this paper, we present an update to its development and explore its application to the study of HIRIS system parameters.

Several enhancements to this model have recently been made. The model has been augmented by the implementation of LOWTRAN 7 (Kneizys, et. al. 1988) for the atmospheric effects. This version now includes multiple scattering in its calculations for the path radiance. The surface reflectance is generated with a multivariate Gaussian distribution from data stored in the LARS Field Database (Biehl, et. al., 1982). The wavelength range has been extended to cover 0.4 - 2.4 μm in 10 nm increments, allowing an implementation of the complete HIRIS model. The processing portion of the model has been enhanced by the addition of a spectral feature compression scheme (Chen and Landgrebe, 1988).

The application of the system model to studying HIRIS performance was chosen for this paper because this instrument represents the near-term state of the art in the complexity of remote sensing systems, and can help provide insight into the process of remote sensing.

2. REMOTE SENSING SYSTEM MODEL

The context that has been used for this model has been one of studying land use in agricultural areas with multispectral sensors covering the optical spectrum. The output of the system model is a classification accuracy of the simulated imagery.

The scene is generated by first creating a spectral reflectance array consisting of vectors representing the reflectance across the spectrum at each spatial location. These reflectance vectors are arranged by class and are spatially correlated through the use of a two-dimensional autoregressive model. The atmospheric effects process is then applied using LOWTRAN 7 to create a spectral radiance function that represents the radiance incident upon the sensor.

The sensor model then takes this function and samples it spatially and spectrally according to its parameters. Electrical noise is then added in before a conversion to a digital number occurs and a digital multispectral image is produced.

The processing portion of the simulator then performs an optional data compression function before classifying the image according to the maximum likelihood

¹ The work reported in this paper was funded in part by NSF Grant ECS 8507405

algorithm. The classification accuracy is then computed by comparing the classified image to the original scene definition.

3. HIRIS MODEL

A block diagram of the HIRIS model as implemented in the system simulation is shown in Figure 1.

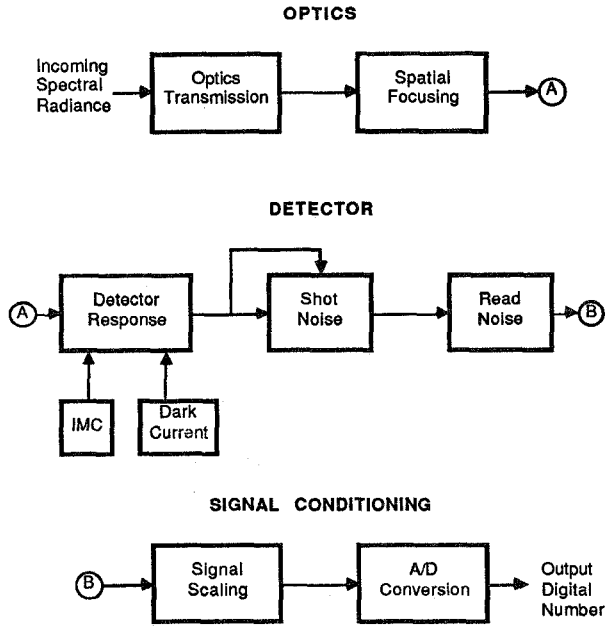


Figure 1. HIRIS Model Block Diagram

This block diagram includes most major spatial, spectral, and radiometric effects in the instrument. The data used for the various parts of the model were obtained from a Jet Propulsion Laboratory report (JPL, 1987) and the paper by Goetz and Herring, (1989).

In many Earth resource analysis applications, the output measure is some form of classification map of the observed area. The classification is usually obtained by a computer algorithm that uses the mean and covariances of the multispectral image data to distinguish between the classes. Thus, in this application not only are signal levels important, but so are signal power variations.

To gain a more realistic sense of how the system noise levels affect HIRIS performance, two versions of Signal-to-Noise Ratio (SNR) are defined: Voltage SNR, and Power SNR. These are defined for each spectral wavelength band m as in equations (1) and (2).

$$\text{Voltage SNR}_m = 20 \log_{10} \left\{ \frac{\bar{P}_m G_m}{\sqrt{\sigma_{\text{shot},m}^2 + \sigma_{\text{read},m}^2 + \sigma_{\text{quant}}^2}} \right\} \quad (1)$$

$$\text{Power SNR}_m = 10 \log_{10} \left\{ \frac{\sigma_m^2 G_m^2}{\sigma_{\text{shot},m}^2 + \sigma_{\text{read},m}^2 + \sigma_{\text{quant}}^2} \right\} \quad (2)$$

where,

- \bar{P}_m = Mean surface reflectance at wavelength band m
- σ_m^2 = Variance of surface reflectance at wavelength band m
- G_m = Conversion factor with units of number of electrons due to the solar irradiance at the surface, atmospheric transmittance, and the sensor response for wavelength band m
- $\sigma_{\text{shot},m}^2$ = Variance of shot noise in wavelength band m
- $\sigma_{\text{read},m}^2$ = Variance of read noise in wavelength band m
- σ_{quant}^2 = Variance of quantization noise

4. RESULTS

To study HIRIS noise and classification performance, the baseline system configuration shown in Table 1 was defined. These parameters were used along with typical vegetation reflectance data to produce the SNR plots shown in Figure 2.

Meteorological Range	16 Km
Solar Zenith Angle	30°
View Zenith Angle	0°
IMC Gain State	1
Sensor Noise Levels	Nominal
Radiometric Resolution	12 bits

Table 1. Baseline System Configuration

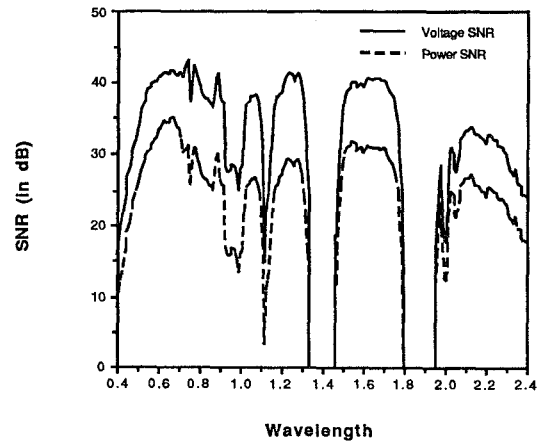


Figure 2. Voltage and Power SNR for typical vegetation

To study the classification performance of HIRIS, a test scene was defined containing three classes from a Kansas Winter Wheat data set (from May 3, 1977), and the baseline system configuration of Table 1. The classification of the simulated images was done using 16 features. These features were the result of combining several wavelength bands together according to the algorithm described in Chen and Landgrebe, (1988). The resulting classification accuracy is the average of the three class accuracies.

Figure 3 presents the results of a study on the relationship of the Image Motion Compensation (IMC) gain state, and the atmospheric meteorological range. The accuracies are the average of five runs of the simulation.

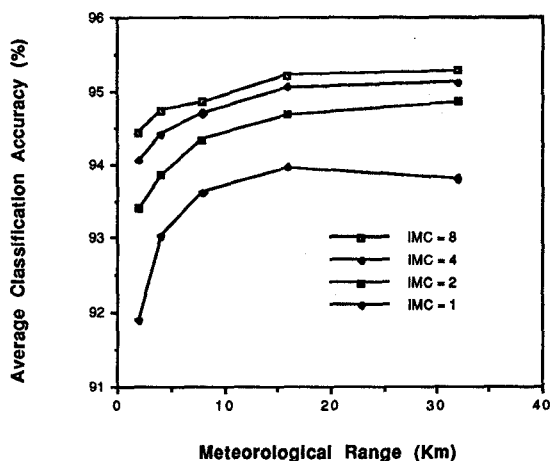


Figure 3. Effect of IMC on Classification Accuracy vs. Meteorological Range

From this result one can see that even in clear atmospheres the classification accuracy is increased for higher IMC states. One can also see that the improvement is greatest for hazy atmospheres. Thus, for the noise levels used in the simulation the increase in signal level of the higher IMC states dominates the corresponding increase in received path radiance and resulting shot noise, thus allowing a higher classification accuracy.

One significant part of the real instrument not included in the model of Figure 1 is error in radiometric calibration. This omission is mainly due to the fact that adequate data does not exist to develop a model for this error. To test the significance of this omission, a model of the error based on percentage of value, and distributed uniformly with a mean of zero, was inserted before the signal conditioning. This error is distributed randomly across the image and represents a relative error. Figure 4 shows the effect of this error as it varies over the range of 0.0 to 4.0 percent.

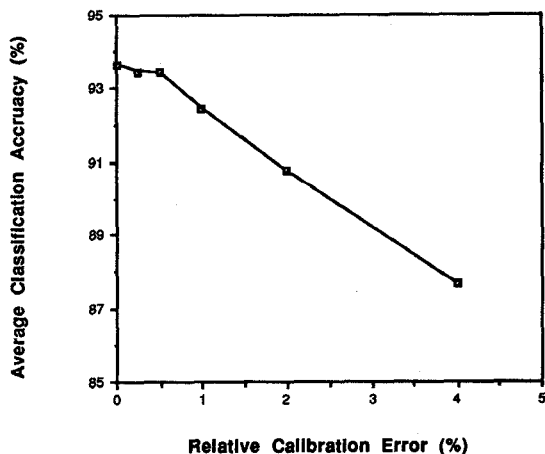


Figure 4. Accuracy vs. Relative Calibration Error

This model for calibration error shows a significant effect for errors on the order of one percent of value or greater, and shows the importance of accurate relative calibration.

To investigate the relationship between SNR and classification accuracy, several experiments were run under different system configurations. To compute the voltage SNR for the entire feature set, the signal levels and the noise levels of the wavelength bands were simply added together. In computing the power feature SNR, the crossband correlation of the reflectances was used to combine the signal levels, while the noise levels were again just added together. Ten repetitions of the simulation results were averaged and the scatter plot of Figure 5 was produced.

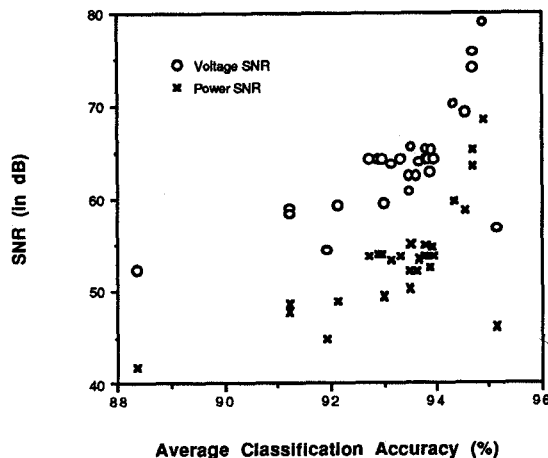


Figure 5. Classification Accuracy vs. Combined Feature SNR.

Attempts to fit a linear or polynomial equation to these plots yielded a correlation coefficient of 0.7 for the best fit, that being a 3rd order polynomial. While there is a general relationship here between SNR and classification accuracy, they appear to be loosely correlated at best.

Next, several sets of six features (shown in Table 2) were used to compare their classification performance. The SFD features were derived from the reflectance statistics by using the algorithm of Chen and Landgrebe, (1988). The SNR features were chosen based upon wavelength regions of high SNR. Figure 6 shows the combined SNR for the various feature sets, while Figure 7 shows the resultant classification accuracy for the baseline image used in this report.

Feature	SFD	TM	WSNR	NSNR	SSFD	SSNR
1	0.42-0.66	0.45-0.52	0.40-0.70	0.51-0.56	0.59	0.54
2	0.66-0.84	0.52-0.60	0.77-0.90	0.81-0.86	0.75	0.84
3	0.70-0.92	0.63-0.69	1.00-1.10	1.02-1.07	0.81	1.04
4	1.48-1.64	0.76-0.90	1.15-1.30	1.20-1.25	1.56	1.11
5	1.98-2.20	1.45-1.75	1.50-1.74	1.59-1.64	2.10	1.61
6	2.20-2.40	2.08-2.35	1.97-2.40	2.16-2.21	2.30	2.19

Table 2. Wavelength bands (in μm) combined for the various feature sets. The feature sets are named as SFD = Spectral Feature Design algorithm (ref. 2), TM = Landsat Thematic Mapper, WSNR = Wide Signal-to-Noise Ratio, NSNR = Narrow Signal-to-Noise Ratio, SSFD = Single band Spectral Feature, SSNR = Single band Signal-to-Noise Ratio.

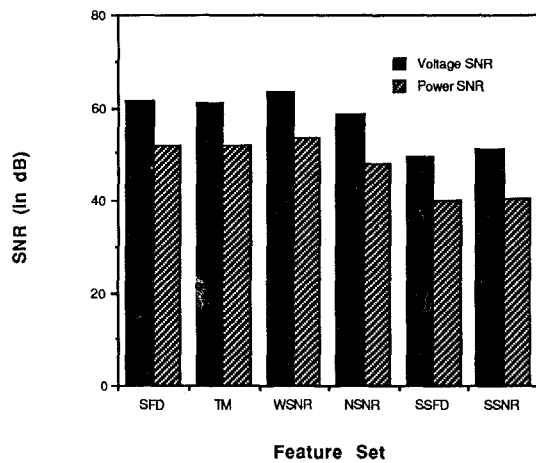


Figure 6. SNRs for the various feature sets.

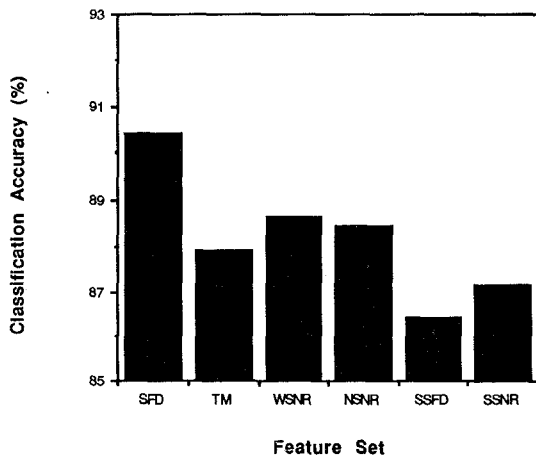


Figure 7. Classification accuracy for the various feature sets.

The features derived from the SFD algorithm performed the best, even though they did not have the highest signal-to-noise ratios.

5. CONCLUSIONS

The results of this work suggest an understanding of the various parameters and their effects to be an important tool in using the configurable instruments of the future. The simulation has been helpful in exploring the SNR performance of HIRIS, and in showing how various feature sets can affect classification accuracy. The importance of accurate relative calibration was also pointed out. While much work remains to be done, these results show the effectiveness of exploring system operation and performance through modeling and simulation.

6. REFERENCES

1. Biehl, L.L., M.E. Bauer, B.F. Robinson, C.S.T. Daughtry, L.F. Silva, and D.E. Pitts, "A Crops and Soils Data Base for Scene Radiation Research," *Proceedings of the 8th International Symposium on Machine Processing of Remotely Sensed Data*, pp. 169-177, Purdue University, West Lafayette, IN, 1982.
2. Chen, C.-C., and D.A. Landgrebe, "A Spectral Feature Design System for High Dimensional Multispectral Data," *Proceedings of IGARSS '88 Symposium*, pp. 891-894, Edinburgh, Scotland, 13-16 September 1988.
3. Goetz, A.F.H., and M. Herring, "The High Resolution Imaging Spectrometer (HIRIS) for Eos," *IEEE Transactions on Geoscience and Remote Sensing*, Vol. GE-27, No. 2, pp. 136-144, March 1989.
4. JPL, "High-Resolution Imaging Spectrometer (HIRIS): Phase A Final Report," JPL D-4782, Jet Propulsion Laboratory, California Institute of Technology, Pasadena, CA, November 1987.
5. Kerekes, J.P. and D.A. Landgrebe, "Simulation of Optical Remote Sensing Systems for Earth Resource Analysis," in *Proceedings of IGARSS '88*, pp. 1211-1214, Edinburgh, Scotland, 13-16 September, 1988.
6. Kneizys, F.X., et. al., "Atmospheric Transmittance/Radiance Computer Code LOWTRAN 7," AFGL-TR-88-0188, Air Force Geophysical Lab, Bedford, MA, August 1988.
7. Salomonson, V.V., et. al., "MODIS: Advanced Facility Instrument for Studies of the Earth as a System," *IEEE Transactions on Geoscience and Remote Sensing*, Vol. GE-27, No. 2, pp. 145-153, March 1989.